Robert Tonndorf, Elke Gossla, Recep Türkay Kocaman, Martin Kirsten, Rolf-Dieter Hund, Gerald Hoffmann, Dilbar Aibibu, Michael Gelinsky, Chokri Cherif

Factors affecting the mechanical and geometrical properties of electrostatically flocked pure chitosan fiber scaffolds

Erstveröffentlichung in / First published in:

Textile Research Journal. 2018, 88(17), S. 1965 – 1978 [Zugriff am: 07.08.2019]. SAGE journals. ISSN 1746-7748.

DOI: https://doi.org/10.1177/0040517517715083

Textile Research Journal

Original article

Textile Research Journal
2018, Vol. 88(17) 1965–1978

DOI: 10.1177/0040517517715083
journals.sagepub.com/home/trj
SAGE

Factors affecting the mechanical and geometrical properties of electrostatically flocked pure chitosan fiber scaffolds

Robert Tonndorf[1], Elke Gossla[2], Recep Türkay Kocaman[1], Martin Kirsten[1], Rolf-Dieter Hund[1], Gerald Hoffmann[1], Dilbar Aibibu[1], Michael Gelinsky[2] and Chokri Cherif[1]

Abstract

The field of articular cartilage tissue engineering has developed rapidly, and chitosan has become a promising material for scaffold fabrication. For this paper, wet-spun biocompatible chitosan filament yarns were converted into short flock fibers and subsequently electrostatically flocked onto a chitosan substrate, resulting in a pure, highly open, porous, and biodegradable chitosan scaffold. Analyzing the wet-spinning of chitosan revealed its advantages and disadvantages with respect to the fabrication of the fiber-based chitosan scaffolds. The scaffolds were prepared using varying processing parameters and were analyzed in regards to their geometrical and mechanical properties. It was found that the pore sizes were adjustable between 65 and 310 μm, and the compressive strength was in the range 13–57 kPa.

Keywords

chitosan fiber, wet spinning, electrostatic flocking, mechanical properties, flock scaffold

The hyaline cartilage at the articular ends of bones exhibits little to no intrinsic self-repair capacity in the face of damage, which may cause osteoarthritis. Current cartilage defect treatments in clinical practice are microfracture (perforation of the bone), mosaicplasty (transplantation of autogenous osteochondral grafts from non-weight-bearing areas to the site of the defect), and autologous chondrocyte implantation (implantation of hyaline tissue cultured from patient cells).[1,2] Within the last two decades the interdisciplinary research field of tissue engineering (TE) has developed rapidly. The objective is to further improve treatments of cartilage defects,[2–4] and therefore three key components are under investigation: cells, signals, and scaffolds.[2,3] Scaffolds are applied as a template for tissue formation; for this purpose they are seeded with cells and growth factors if required. Subsequently, mechanical, chemical, and biological stimuli are utilized to guide and influence tissue formation within the scaffold–tissue constructs.

Great efforts have been made in scaffold preparation. Hutmacher proposed the following criteria of scaffold–tissue constructs: (1) interconnected pores in a three-dimensional network; (2) controllable degradation and resorption rates to match tissue growth; (3) surface chemistry suitable for attachment, proliferation, and differentiation of cells; and (4) mechanical properties similar to the tissues at the implantation site.[5] Several natural and synthetic polymers have been investigated for scaffold preparation, including chitosan,[6,7] which is a linear polysaccharide, a deacetylated derivative of chitin, and is isolated from crab and shrimp shells.[8] It is supremely suited for TE,[7,9] especially for cartilage TE applications,[10] as its advantages over other biopolymers are its biodegradability

[1]Institute of Textile Machinery and High Performance Material Technology, Technische Universität Dresden, Germany
[2]Centre for Translational Bone, Joint and Soft Tissue Research, University Hospital and Medical Faculty, Technische Universität Dresden, Germany

Corresponding author:
Robert Tonndorf, Institute of Textile Machinery and High Performance Material Technology, Hohe Straße 6, Dresden 01069, Germany.
Email: robert.tonndorf@tu-dresden.de

into non-toxic oligosaccharides, its similarity to glycosaminoglycans in the extracellular matrix, and its hydrophilic surface, promoting cell adhesion and proliferation.

Commonly used methods for the fabrication of two- and three-dimensional scaffolds are freeze-drying, phase separation, salt leaching, cell encapsulation, gas forming, and electrospinning,[11–15] as well as bubbfil and centrifugal spinning.[16] Likewise, textile technologies are a suitable approach for a fiber-based scaffold fabrication, considering that with these technologies structural, topographical, and mechanical properties of the constructs are widely adjustable. The most common techniques applied for textile scaffold preparation are weaving, knitting, braiding, nonwoven technologies, and electrospinning.[17,18] Moreover, electrostatic flocking technology has been used for the preparation of three-dimensional anisotropic scaffolds, featuring a columnar fiber orientation to enhance the biomechanical properties under compression.[19–23] Gossla and colleagues recently prepared flocked scaffolds consisting of chitosan only, ensuring full biodegradability.[24] It was found that these scaffolds were suitable for the proliferation of hMSC and Saos-2 cell lines, hence they were proposed as a promising candidate for articular cartilage TE applications.

In this work, the possibilities and limitations of applying wet-spun chitosan yarns in electrostatically flocked chitosan fiber scaffolds will be shown. Therefore, the chitosan spinning process is characterized regarding the drawing process and its impact on the wet tensile properties of the chitosan yarns, as no data are available in the literature, despite its importance as a parameter, especially when soaking chitosan fibers in an aqueous solution for TE applications. The following geometrical properties of prepared scaffolds are examined as well: the flock fiber density, the surface-area-to-volume ratio (SA:V), the porosity and the pore size, and the compressive strength. The obtained data will be used for a comparison to pure three-dimensional chitosan scaffolds described in the literature.

Experimental details

Materials

Two chitosan (CHS) types, Chitoscience CHS 95/100 and CHS 95/500, were purchased from Heppe Medical Chitosan GmbH (Halle, Germany), each having a degree of deacetylation (DD) greater than 92.6% and a viscosity of 71–150 mPa (CHS 95/100) and 351–750 mPa (CHS 95/500), measuring a 1% CHS solution in 1% acetic acid, as stated by the supplier. The types were chosen for their high DD, which decreases degradation rates and increases the number of cell attachment sites.[25,26] The molecular weight (MW) of CHS 95/100 was between 100,000 and 250,000 g/mol, and for CHS 95/500 was between 200,000 and 400,000 g/mol, as stated by the supplier. CHS 95/100 was used for fiber formation and CHS 95/500 was used for adhesive and substrate formation of the scaffolds. The higher MW of the latter was chosen to ensure a slower degradation rate of the fiber-supporting substrate, as the MW of CHS is inversely proportional to its degradation rate.[25] Acetic acid (AcOH), sodium hydroxide (NaOH), and Dulbecco's phosphate buffered saline without calcium and magnesium (PBS) were purchased from Merck KGaA (Darmstadt, Germany).

Wet-spinning of chitosan filament yarns

Wet-spinning of chitosan filament yarns was conducted on an in-house wet-spinning pilot plant provided by Fourné Polymertechnik GmbH (Alfter, Germany) in accordance with Toskas and colleagues and Hild and colleagues.[27,28] The spinning dope was prepared by mixing at least 3 L of an aqueous solution containing 8 wt.% CHS 95/100 and 2.8 1 wt.% AcOH in demineralized water, stirring for 5–8 h in a dissolver and aging for 24 h. Subsequent filtration through a filter from Paul GmbH & Co. KG (Steinau an der Straße, Germany) consisting of three layers with a pore size of 50 µm removed non-dissolved components from the chitosan solution.

The filtered spinning dope was heated to a temperature of 60°C, extruded through a spinneret and coagulated in an aqueous alkaline bath at 50°C and a pH value of 12.6. Subsequently, the yarn was continuously passed through three additional alkaline baths with decreasing temperatures (50°C, 45°C, and 40°C) and pH values (10.6, 9.7, and 9.7). The pH of the baths was adjusted by adding NaOH. The spinneret pressure was typically about 5 bar. Finally, the yarn was passed through a godet dryer with a 40 m drying path and a temperature of 100°C, before being wound onto a coil. Yarn withdrawal from the baths and from the oven was achieved by five godets and one additional godet just before winding, resulting in a total of six drawing sections. The drawing rate was determined by the ratio of the take-up speed of the godets and the extrusion velocity of the dope at the spinneret. The total drawing rate was the ratio between the last godet and the extrusion velocity.

Yarns with a nominal single filament diameter of 25, 40, and 50 µm were spun for scaffold preparation. Therefore, calculations were performed, assuming a constant volumetric flow rate of chitosan (Eqs. 1.1–1.6). Microsections of dry chitosan yarn samples were recorded with an Axiotech 100 optical microscope by

Zeiss (Oberkochen, Germany) and the diameter was measured and compared to the nominal diameter.

Mechanical analysis of chitosan yarns

The linear mass density related tensile strength and Young's modulus of wet and dry chitosan yarn samples were obtained as a function of the total drawing rate. The tensile properties of the samples were measured on a Z2.5 tensile tester with a 100 N load cell by Zwick (Ulm, Germany), based on the DIN EN ISO 2062 standard. Dry yarn samples were conditioned at 20°C and 65% relative humidity. Wet yarn samples were immersed in a PBS solution for 24 h and then directly tested without drying. Prior to the tensile tests, the linear mass density of the yarns was determined to calculate the tensile strength in cN/tex. The gauge length was 250 mm and the extension rate was 250 mm/min. The values from tensile testing were analyzed with the software testXpert I and were averaged by means of at least 10 samples.

Fabrication of scaffolds

Scaffolds were prepared by electrostatic flocking as described by Gossla and colleagues.[24] Flocking from bottom to top was achieved using an electrostatic flocking device (SPG 1000 from Maag Flockmaschinen GmbH, Kusterdingen, Germany), which consisted of a circular top electrode (area 26.42 cm^2) and a circular bottom electrode (area 67.93 cm^2) made of aluminum alloy and set apart at a distance of 10 cm. The surface of the top electrode was roughened by partial dissolution with 0.1 M NaOH and subsequently thoroughly rinsed with water. This procedure ensured that the adhesive film was distributed evenly on the electrode, which would not have been possible using a non-treated electrode. The chitosan yarn was cut into flock fibers with a set length of 2 mm on a cutting machine built in-house. This fiber length corresponded to the thickness of the articular cartilage.[29] The flock fiber length in dry and in wet states was measured with an Axiotech 100 optical microscope by Zeiss.

Various set parameters for scaffold fabrication were applied, resulting in 10 differently prepared scaffold types (Table 1), whereby the flock fiber weight (G, H, I and O, Q, R), the voltage (E, F, G), and the fiber diameter (H, M, O) was varied. Type N and P were prepared to achieve a high compressive strength, hence a low voltage (30 kV) and a high fiber diameter (50 μm) was applied. Prior to flocking, flock fibers were dried at 120°C for 5 min to ensure the separability of hydrophilic fibers. These fibers were then homogeneously distributed on the bottom electrode by means of a mechanical sieve from Maag Flockmaschinen GmbH. A thin layer of the chitosan adhesive (1 g of an aqueous solution containing 5 wt.% CHS 95/500 and 5 wt.% AcOH) was evenly distributed on the top electrode by knife coating. By applying a voltage, the flock fibers on the bottom electrode were accelerated toward the top electrode and adhered to the applied chitosan adhesive. During this process the temperature was 22°C and the relative humidity was 39%.

The as-prepared structures were thermally cured at 120°C for 15 min, whereby the adhesive was converted into a thin film and substrate, respectively. Finally, the scaffold was neutralized in a freshly prepared 0.1 M NaOH solution (90/10 vol.% ethanol/water, 20 ml), and subsequently immersed in 100% ethanol for 1 h and then air-dried. Ethanol-based solutions enabled drying without substrate deformation, as alcohol dehydrates chitosan and therefore swelling and succeeding deformation was omitted.

Microscopy/gravimetry-based geometrical analysis of scaffolds

The flock fiber length in dry and in wet states as well as the flock fiber diameter in the wet state were determined by microscopy-based measurements. For wet fiber dimensions, fiber samples were incubated in PBS for 24 h and stained with an acid dye (Säurelicht-rot B from Chemie GmbH Bitterfeld Wolfen, Bitterfeld Wolfen, Germany). Dry and wet samples were then distributed in glycerine and images of the fibers in longitudinal view were recorded with an Axiotech 100 optical microscope by Zeiss. Measurements of at least 10 fiber samples were conducted and both dimensions were averaged.

The yield of fiber flocking and the geometrical parameters of the scaffold types in dry and in wet states were calculated using gravimetry-based measurements

Table 1. Set parameters for scaffold preparation

Scaffold type	E	F	G	H	I	M	N	O	P	Q	R
Voltage (kV)	30	40	45	45	45	45	30	45	30	45	45
Set flock fiber mass (g)	0.5	0.5	0.25	0.5	1.0	0.5	0.5	0.5	1.0	0.25	1.0
Set flock fiber diameter (μm)	25	25	25	25	25	40	50	50	50	50	50

from flocking and microscopically determined fiber diameters (Eqs. 2.1–2.8). Calculated parameters were the flock fiber density, the SA:V, the porosity parallel to the plane of the chitosan film, and the pore size. For pore sizes the assumption was made that the flocked fibers were packed uniformly in a hexagonal packing arrangement. For averaged values and standard deviation, five scaffolds of each type were investigated.

Microscopy-based geometrical analysis of scaffolds

Complementary to the gravimetric analyses, the flock fiber density and the distance between fibers of the flocked scaffolds were determined by means of microscopic evaluation. To this end, samples were stained with a 20 g/L Alizarin red S (Sigma) solution and subsequently embedded in a 150 g/L gelatin (Fluka) solution. The samples were frozen in liquid nitrogen and stored at –80°C before cryosectioning. Cryosections were observed under a light microscope. Based on these sections, the fiber density was calculated as the mean number of fibers per square millimeter. The distance between fibers was defined as the average distance between the centers of a fiber and its nearest neighbors connected by an edge in a Delaunay triangulation. For this purpose, representative images of the cross-sections were analyzed by performing a Delaunay triangulation using the Delaunay Voronoi plug-in of the software Fiji.[30] For the calculation, only fibers within 200 µm from the margin of a detailed image at 1860 × 1240 µm were considered. For each scaffold sample, three cross-sections were analyzed.

Mechanical analysis of scaffolds

The prepared scaffolds were compressed by a maximum deformation ratio of 50% over the wet fiber length. The compressive strength as a function of the rate of deformation was determined on a Z2.5 tensile tester by Zwick. At least three scaffolds of each type were conditioned in PBS for 24 h. Then, each scaffold was cut into six square samples (15 × 15 mm) and swollen samples were submitted to compressive testing. The initial load was set to 0.1 N and the compression rate was set to 5 mm/min.

For the sake of clarity, the compression curves were sectioned into three zones separated by a deformation ratio of 12.5, 25, and 50%. For each zone the averaged maximum compressive strength was shown for differently prepared scaffold types. Walther and colleagues presented how flocked structures undergo Euler buckling when compressed.[19] Hence, the compressive strength at different deformation ratios was compared to Euler's critical load, which was calculated via geometrical parameters (Eq. 3).

Elemental analysis of scaffolds

As pure chitosan scaffolds were the intended goal, the chitosan fibers and the adhesive were characterized by their content of AcOH before and after certain washing steps, as AcOH was the only organic compound added during the fabrication process with potentially cytotoxic effects.[31,32] As-spun fiber samples and the adhesive, which was cured at 120°C for 5 min, were defined as unwashed, whereas washed samples were treated with two different washing procedures. For washing procedure 1, samples were first neutralized in 0.1 M NaOH for 1 h and subsequently washed in demineralized water for another 1 h. These samples served as a reference. For washing procedure 2, samples were neutralized in a freshly prepared 0.1 M NaOH ethanol-based solution (90/10 vol.% ethanol/water) for 1 h and subsequently washed in 100% ethanol for another 1 h, which corresponded to the actual scaffold fabrication. For AcOH determination the weight ratio of carbon (C) to nitrogen (N) was assumed to be proportional to the AcOH concentration within the fibers and the substrate. This weight ratio was determined twice on air-dried samples with a Euro EA – CHNSO Elemental Analyser from HEKAtech GmbH (Wegberg, Germany). The obtained C/N ratios were compared with theoretical ratios, which were calculated based on the DD of chitosan and the amount of AcOH added.

Results and discussion

Wet-spinning of chitosan filament yarns

In spinning experiments, the total drawing rates were varied between 0.5 and 1.3, and for each rate several hundred meters of yarn were spun. It was found that the ratios between the drawing rates at a given godet ($DR_1 \ldots DR_6$) and the total drawing rates (DR_6) were similar for all spinning experiments. The averaged ratios and the corresponding coefficients of determination are given in Table 2. The values from this table were calculated according to mathematical functions of the linear regression lines (Figure 1a). Drawing occurred primarily within the coagulation bath between the spinneret and the first godet, which is represented by the drawing rate ratio DR_1/DR_6 having a value of 74%. About 93% of the total drawing was achieved after passing the second godet, and almost no drawing occurred at godets 3–6. Drawing rates substantially differing from those in Table 2 were not suitable for yarn production as they either resulted in breaking or sagging of the water-swollen filament yarn. Hence, the total drawing rate was determined by exclusively considering the drawing rate within the coagulation bath. By applying the mathematical functions shown in

Figure 1a, the take-up speeds of the godets are preconfigurable according to the required total drawing rate. For the sake of completeness, total drawing rates exceeding 1.3 were not applicable as the yarn broke before final winding.

The single-filament diameter of the as-spun yarn was a crucial parameter for scaffold preparation. The diameters were optically measured and compared with the calculated nominal diameter. Both values corresponded, as seen in Figure 1b. Thus, it was shown that wet-spun chitosan fibers are suitable for the preparation of geometrically well-defined chitosan scaffolds, as the diameter is easily controllable.

In conclusion, only two set parameters, more precisely the diameter of the spinneret and the first applied drawing rate, were required as an input, making the described wet-spinning a straightforward method for the provision of chitosan fibers with predefined diameters.

Mechanical analysis of chitosan yarns

Drawing of chitosan yarns affects the polymer orientation and therefore the tensile properties.[33,34] In the literature it is not clarified whether there is a relationship between drawing and the tensile properties of wet chitosan filament yarns. For the as-spun and dry chitosan yarns, a linear correlation between the drawing rate and the tensile strength (Figure 2a) as well as Young's modulus (Figure 2b) was noticed. Neither correlation proved to be as significant as expected, which was attributed to the production of chitosan from natural resources and thus the chitosan raw material not having homogeneous properties. However, an increased drawing rate generally resulted in an increased tensile strength and Young's modulus.

As the yarn was utilized in scaffolds, the wet tensile properties were of greater interest. Swollen yarn samples were subjected to tensile tests, revealing their tensile properties under physiological conditions in the wet state. To facilitate a wet/dry comparison, the wet and the dry tensile properties were both based upon the dry linear mass densities. The obtained data indicated a large drop in the tensile strength and Young's modulus in the wet state. The most significant changes occurred for highly drawn yarns. Moreover, the dependence between the tensile strength and the drawing rate in the wet state was less pronounced when compared to the dependence in the dry state, and no linear correlation between the drawing rate and the wet Young's modulus was noted (Figure 2). The wet modulus averaged 0.73 ± 0.18 GPa, which was between 4% and 14% of the dry modulus.

A high swelling factor of 2.4 ± 0.2 was determined, which was calculated from the ratio of the linear mass density in wet and dry states. Water interacts strongly with the hydroxyl and amine groups of chitosan, causing swelling and a decrease of intermolecular forces and hydrogen bonds, respectively, between polymer chains,

Table 2. Averaged ratio of drawing rate at each godet DR_i to total drawing rate DR_6. Averaged ratios were determined from the slope of linear regression lines for the data points (DR_i, DR_6) of 26 spinning experiments; see Figure 1a

i	1	2	3	4	5	6
DR_i/DR_6 (%)	74	93	97	98	99	100
Coefficient of determination	0.93	0.99	1	1	1	1

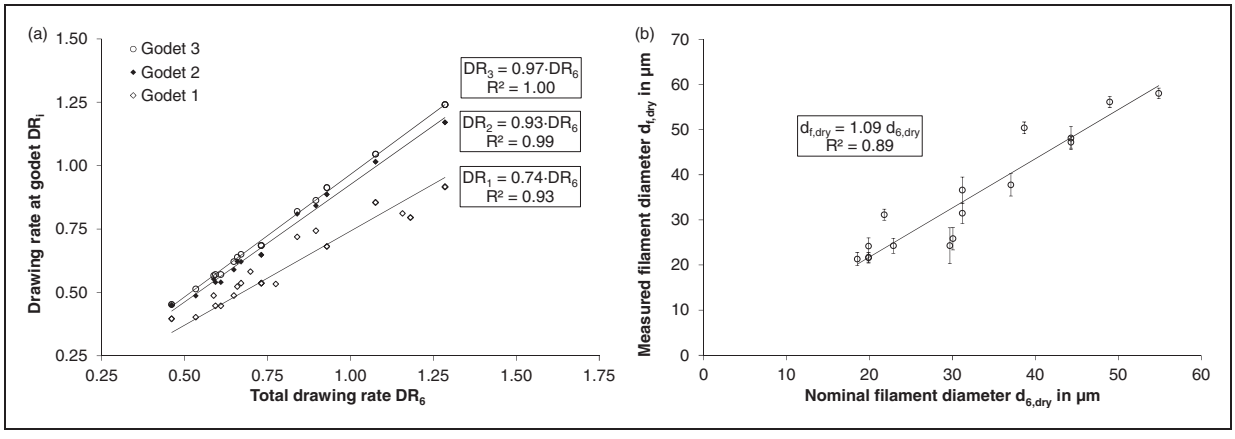

Figure 1. (a) Drawing rate at the first three godets plotted against the total drawing rate. (b) Measured filament diameter plotted against the calculated filament diameter.
Error bars represent standard deviation for 10 samples for each nominal diameter; coefficient of determination (R^2) for linear regression.

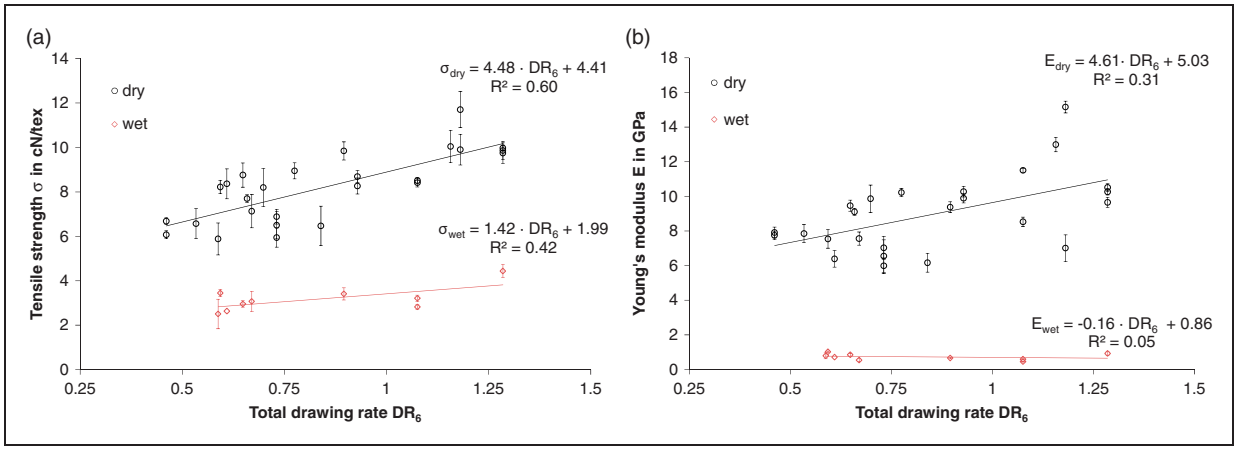

Figure 2. (a) Tensile strength and (b) Young's modulus plotted against total drawing rate.
Error bars represent standard deviation for 10 samples for each yarn. Coefficient of determination (R^2) for linear regression are given.

resulting in decreased wet strength. Furthermore, orientation of polymer chains due to drawing is lost as well. Hence, the correlations between the drawing rate and the tensile strength or Young's modulus in the wet state were small or negligible. In conclusion, the wet Young's modulus, which was the essential parameter for the compressive strength of the scaffolds, was not adjustable by drawing.

Geometrical analysis of scaffolds

For scaffold fabrication, three different flock fiber types were used. All fibers had a nominal set fiber length of 2 mm but differing set fiber diameters of 25, 40, and 50 µm. For all flock fibers the measured fiber length in dry state was less than the set fiber length, which was due to the imperfection of fiber cutting. All three flock fiber diameters in the dry state corresponded to the set diameter. The diameter in the wet state was measured on stained fiber samples (Figure 3a). An increased fiber diameter was noticed due to swelling. Measured dimensions of flock fibers applied for scaffold fabrication are given in Table 3. These values were further used for the calculation of scaffold properties.

Ten different scaffold types with various set fabrication parameters having a diameter of 58 mm were prepared. An overview is given in Table 4. For all scaffolds, a dense and a homogeneous flock surface as well as a vertical orientation of the flock fibers were achieved (Figure 3b,c). A dry substrate weight of 74 ± 4 mg, not including fibers, was measured. Not all initial fibers that were distributed onto the bottom electrode were accelerated and adhered to the adhesive; as a consequence, the flocking yield was in the range 55–85%. As expected, an increased initial fiber weight resulted in an increased fiber density within the scaffold. Decreased flocking voltages led to an increased fiber density, which was probably due to a decreased electrostatic charge of the fibers. This circumstance in turn implied decreased repulsing forces between incoming and adhering fibers, allowing an increased fiber packing density. Furthermore, the thinner the flock fibers were, the higher the flock fiber density became. In general, a broad range of fiber densities from 9 to 113 fibers/mm^2 was achieved. These gravimetrically determined fiber densities were confirmed by microscopic measurements, which revealed densities of 73, 105, and 49 mm^{-2} for the scaffold types H, I, and M.

Certain geometrical parameters in the wet state were calculated based on the combination of gravimetrical and microscopic measurements (Table 4): SA:V was in the range 1.8–12.8 mm. Pore sizes were in the range 65–310 µm, and porosities were in the range 88–97%. Both parameters are discussed further below. By applying the Delaunay triangulation to recorded microscopic images of the scaffolds cross-section (Figure 4), the frequency of discrete fiber distances, from center to center between neighboring fibers, was determined. The frequency distribution shifts to the left, as shown in Figure 4a. The mean fiber distance between neighboring fibers was reduced from 140 ± 9 (Type H) to 112 ± 3 µm (Type I) as the fiber count was increased. The application of a larger fiber diameter (Type M) resulted in an increased fiber distance (145 ± 8 µm) and in a more uneven distribution of the fibers. The averaged values of fiber distances from microscopic analysis and microscopy/gravimetry-based determined distances are similar. Differences occur due to the real fiber distribution of the scaffolds, which is not a hexagonal arrangement as assumed for the microscopy/gravimetry-based measured values. As the fiber flocking implemented within this work was not producing a uniform distribution of vertically aligned fibers, the pore dimensions cannot be reliably determined without

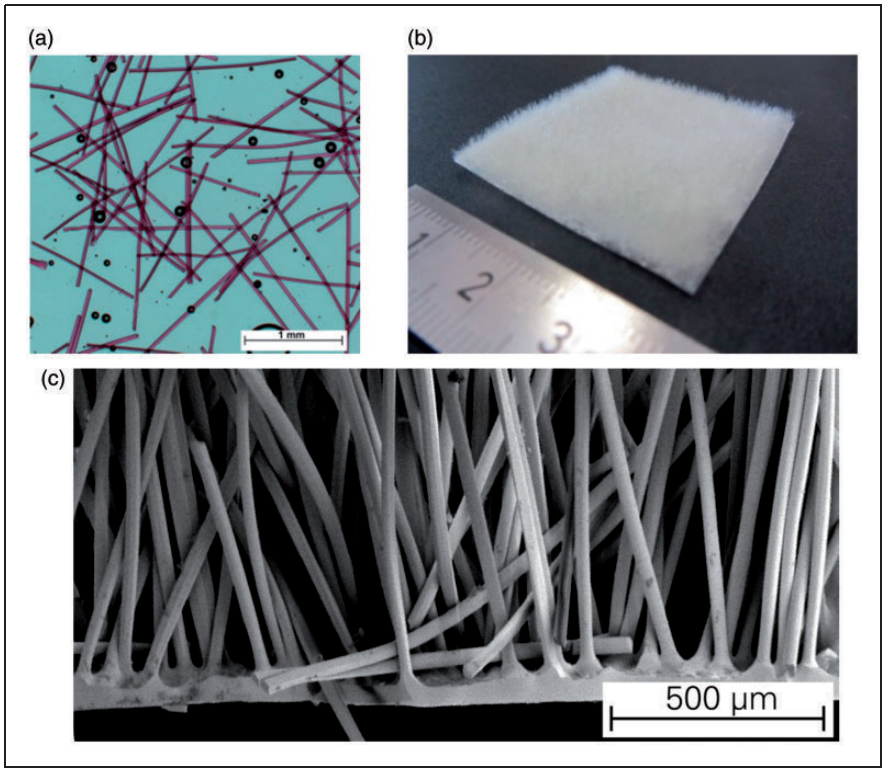

Figure 3. (a) Glycerine-embedded stained flock fibers, (b) cut scaffold sample, and (c) SEM image, bent fibers due to sample preparation/cutting.

Table 3. Overview of microscopy-based determined flock fiber length and diameter in dry and wet states, averaged values with standard deviation

Set flock fiber type Dimension	25 µm/2 mm	40 µm/2 mm Length (mm)	50 µm/2 mm	25 µm/2 mm	40 µm/2 mm Diameter (µm)	50 µm/2 mm
Measurement dry	1.79 ± 0.18	1.82 ± 0.05	1.89 ± 0.05	*25.1 ± 3.2	*39.1 ± 3.5	*50.4 ± 1.3
Measurement wet	1.71 ± 0.13	1.83 ± 0.08	1.91 ± 0.05	38.8 ± 4.5	57.3 ± 6.5	65.2 ± 7.0
Dimensional changes (%)	-4	1	1	55	48	29

*indicates measurements on fibers in transverse view, otherwise in longitudinal view.

Table 4. Overview of microscopy-/gravimetry-based determined geometrical parameters of various scaffold types in the wet state; averaged values with standard deviation for five samples for each type

Scaffold type	E	F	G	H	I	M	N	O	P	Q	R
Set flock fiber type	25 µm/ 2 mm	25 µm/ 2 mm	25 µm/ 2 mm	25 µm/ 2 mm	25 µm/ 2 mm	40 µm/ 2 mm	50 µm/ 2 mm	50 µm/ 2 mm	50 µm/ 2 mm	50 µm/ 2 mm	50 µm/ 2 mm
Fiber density (fibers/mm^2)	113 ± 2	105 ± 19	24 ± 1	80 ± 15	112 ± 19	32 ± 8	28 ± 3	19 ± 2	38 ± 3	9 ± 2	28 ± 3
SA:V (mm)	12.8 ± 0.2	12.0 ± 2.2	3.0 ± 0.1	9.2 ± 1.8	12.7 ± 2.1	6.4 ± 1.5	5.7 ± 0.5	4.2 ± 0.4	7.8 ± 0.63	1.8 ± 0.5	5.8 ± 0.5
Porosity (%)	88.4 ± 0.2	89.2 ± 2.0	97.1 ± 0.1	91.7 ± 1.6	88.6 ± 1.9	90.2 ± 2.3	90.7 ± 0.8	93.1 ± 0.7	87.3 ± 1.0	97.1 ± 0.8	90.6 ± 0.8
Fiber center–center distance (µm)	101 ± 1	106 ± 11	217 ± 5.3	114 ± 17	103 ± 8	190 ± 20	204 ± 9	237 ± 13	174 ± 7	375 ± 63	202 ± 9
Pore size (µm)	65 ± 1	70 ± 11	179 ± 5.3	78 ± 17	67 ± 8	129 ± 20	139 ± 9	172 ± 13	109 ± 7	310 ± 63	137 ± 9

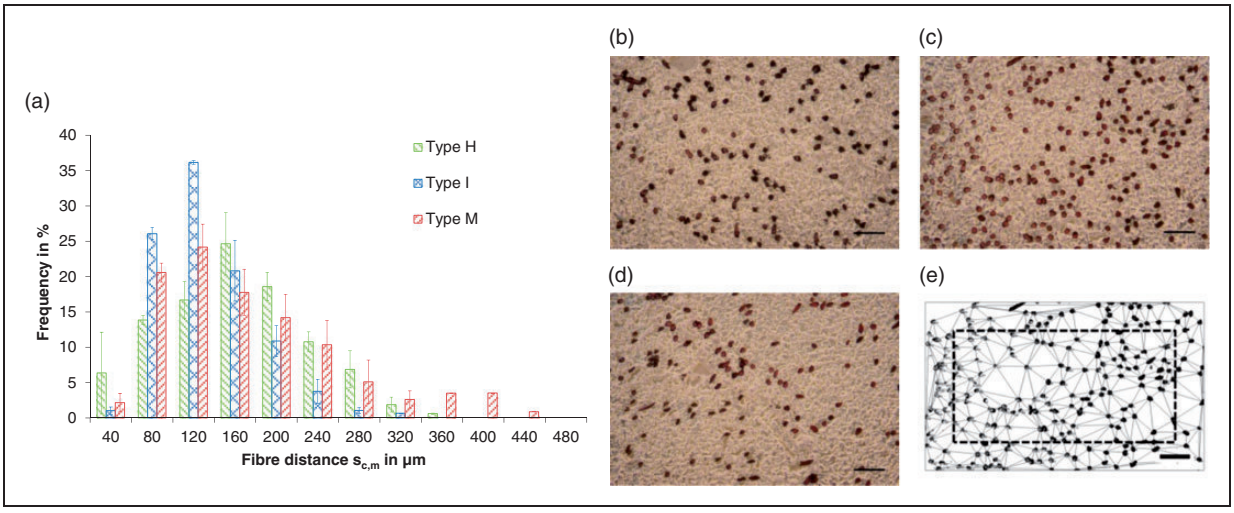

Figure 4. Distribution of fiber distances s_c between nearest neighbors of three chitosan flock scaffolds after applying Delaunay triangulation.
Mean of three flock scaffolds ± SD. Microscopic determination was performed after Alizarin red S staining and cryosectioning (a). Microscopic cross section of scaffold type H (b), type I (c), and type M (d). Representative image for Delaunay triangulation (e). Scale bar = 200 µm.

considering the actual distribution of the fibers. These irregularities led to a higher pore size or fiber distance compared to the calculated values.

Both characteristic parameters – the pore size and the porosity – were proportional, whereas the pore size and the SA:V emerged as being inversely proportional to one another. In general, a high SA:V is desirable to increase the surface for cell adhesion, while it also inhibits the nutrient supply due to small resulting pore sizes. Therefore, one has to make a compromise between optimal pore size and optimal SA:V which allows sufficient adhesion area while still providing efficient exchange of nutrients. The determined parameters of this compromise do not have universal validity, since they need to be adjusted specifically to the chosen scaffold material as well as the needs of the applied cell types. Loh and colleagues gave an overview, wherein scaffolds examined for chondrogenesis exhibited pore sizes in the range 70–860 µm and porosities in the range 59–95%.[11] Listed scaffolds consisted of different materials and were utilized for different cell types. For chondrogenesis within chitosan scaffolds, the porosity was indicated as 80% and the pore sizes were in the range 70–120 µm. Most scaffold types prepared in the presented paper exhibited calculated pores in the same range (except type G, O, and Q) and porosities between 85 and 95%. Hence, the flocked chitosan scaffolds prepared in this work are most likely suitable for cartilage TE applications, as stated by Gossla and colleagues as well, who investigated the scaffold type H regarding the proliferation of hMSC and Saos-2 cell lines.[24]

Mechanical analysis of scaffolds

A representative loading, unloading, and reloading curve of the scaffold type R is shown in Figure 5a, whereas Euler's critical load was calculated as 10 kPa, based on a wet Young's modulus of 0.30 GPa of the yarn, which was calculated with respect to the swollen/wet fiber cross-section. The lower part of the first loading curve (deformation up to 12.5%) was characterized as a left curvature, this may be traced back to fiber buckling within the vertically aligned fiber assembly. The loading stress strongly increased above Euler's critical load, which can most likely be explained by an increased number of fiber–fiber contacts during compacting, as the fibers were densely packed. During fiber compacting, free fiber bending was omitted and the slope of stress progressively increased upon further deformation. Finally, the sharp drop of unloading curves was attributed to the slipping of adjunct fibers.

The evaluation of the obtained stress–strain curves with respect to the succeeding cycles indicated a very small drop of the maximum compressive strength within 10 cycles. However, the loading slopes and the moduli, respectively, decreased with increasing cycle counts, whereby succeeding slopes were approaching a constant value. This was attributed to an irreversible fiber reorientation resulting in a fiber alignment differing from the vertical, which also explained the decreased slopes of the lower part of the reloading curves when compared to the first loading curve. Fiber reassembly is also expressed by the deformation energy, which is the area underneath the loading and

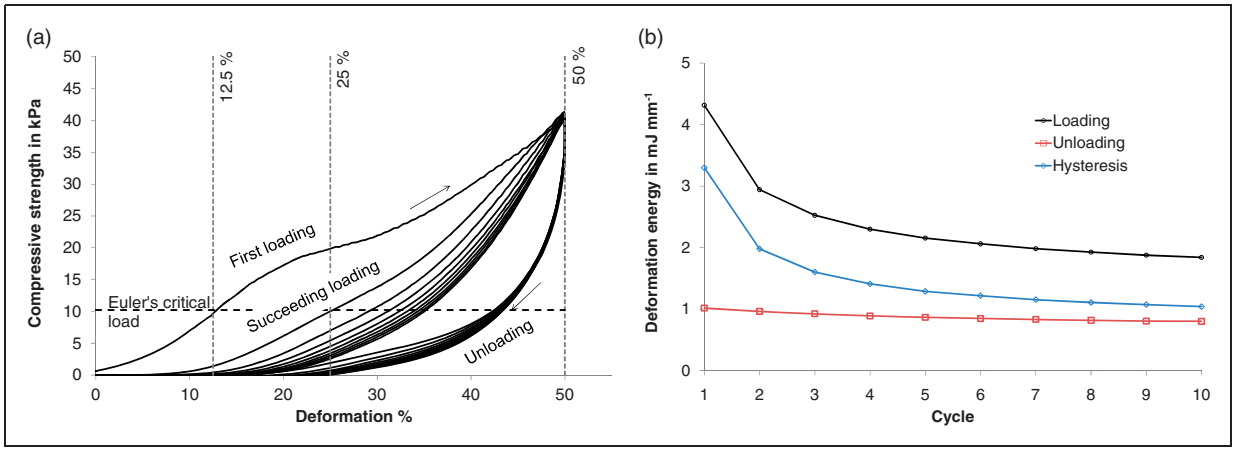

Figure 5. (a) Representative loading, unloading, and reloading curve of a scaffold type R. (b) Corresponding energy of loading, unloading, and hysteresis for each cycle.

Table 5. Compression strength and elastic modulus in kPa of various scaffold types, averaged values with standard deviation

	Compression	H	M	N	O	P	R
Compressive strength	12.5%	2 ± 1	4 ± 3	8 ± 2	6 ± 2	8 ± 1	6 ± 1
	25.0%	5 ± 2	9 ± 6	18 ± 4	10 ± 4	23 ± 4	14 ± 3
	50.0%	13 ± 4	25 ± 10	38 ± 7	23 ± 8	56 ± 6	31 ± 5
Calculation	Euler	5 ± 1	8 ± 2	10 ± 1	7 ± 1	14 ± 1	10 ± 1

the unloading curves. The difference between both deformation energies (hysteresis) was attributed to frictional or dissipated energy between fibers. As seen in Figure 5b, hysteresis was approaching a constant value and thus friction was approaching a constant value as well, which in turn was caused by the manifestation of the reoriented fiber assembly.

For a comparison of the different scaffold types, three averaged stress values, which corresponded to the compression ratios 12.5, 25, and 50%, were chosen (Table 5 and Figure 6). The correlation between these characteristic stress values and Euler's critical load, which was calculated upon the geometrical parameters, was investigated. Only the first loading was considered to ensure an analysis of the vertical fiber assembly. A correlation between Euler's critical load and the compressive strength was ascertained (Figure 6b). As mentioned above, the experimentally determined compressive strength increased above Euler's critical load, which certainly occurred at a deformation of 25%. Although Euler buckling was not applicable at such a high deformation, a correlation was present. It can be presumed that fiber bending during compacting caused this behavior. The applied stress for fiber bending is proportional to the same parameters that are used for the equation of Euler buckling. Hence, the mechanical scaffold analysis showed that the compressive strength of the scaffolds can be approximated from the geometrical parameters, even at high deformation rates.

Still, the mechanical strength of the uncultivated scaffolds is approximately five times lower when compared to the articular tissue, which withstands a compressive strength of 24, 69, 112, and 168 kPa at 8, 16, 24, and 32% cartilage compression.[35] Nevertheless, the mechanical strength of cultivated scaffolds is expected to increase, as embedded cells may form a natural extracellular matrix, which connects the fibers within the scaffold/tissue constructs.

Elemental analysis of scaffolds

Washed and unwashed fibers in addition to adhesive samples were characterized regarding their AcOH content, by assuming that the concentration of AcOH was proportional to the C/N ratio, which was determined by elemental analysis. To enable comparison of the AcOH content at the different preparation stages of the scaffold components, the calculated and the measured C/N ratios were plotted (Figure 7). The calculated values were referred to the source materials: chitosan spinning dope, adhesive, and powder.

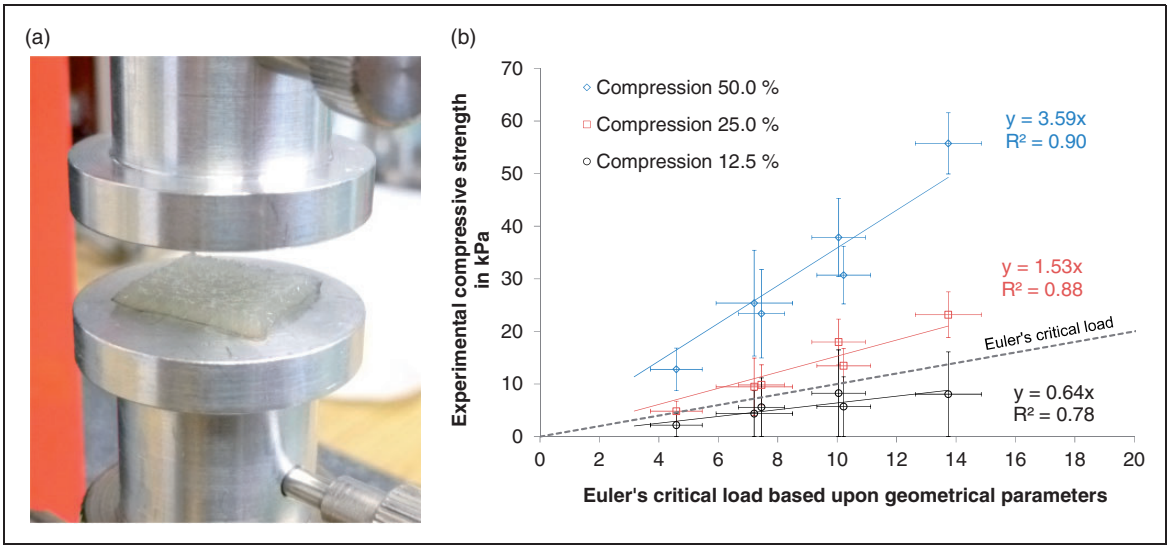

Figure 6. (a) Swollen scaffold sample; square with a side length of 15 mm between clamps for compressive testing. (b) Compressive strength at a compression of 12.5, 25, and 50 % plotted against calculated Euler buckling strength corresponding to the geometrical properties of scaffold types; error bars represent standard deviation for at least 10 samples for each data dot/scaffold type.

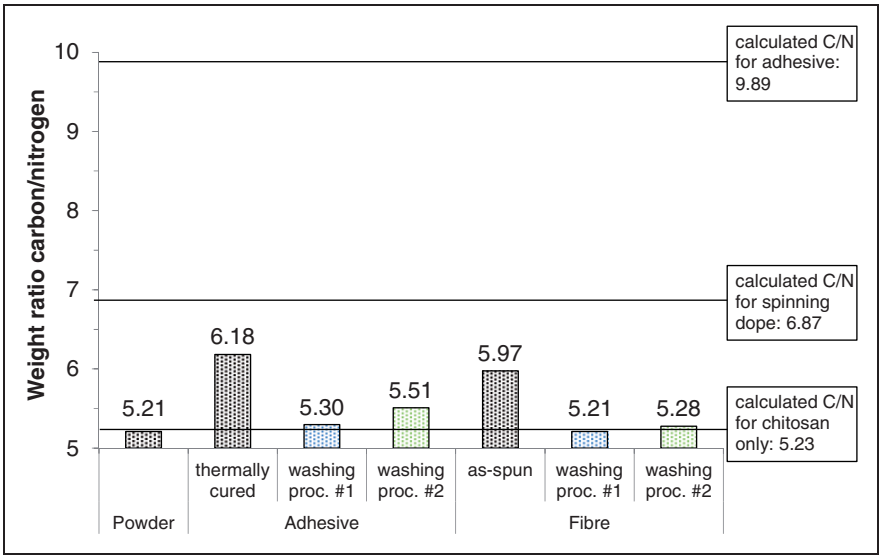

Figure 7. Calculated and measured weight ratios of carbon to nitrogen for various chitosan samples.

The pure powder contained no AcOH and therefore had a low calculated C/N ratio of 5.23; the spinning dope and the adhesive contained AcOH and thus high C/N ratios of 6.87 and 9.89, respectively, were calculated. A high proportion of AcOH evaporated due to the thermal treatment at 120°C for 15 min. However, the measured C/N ratio was still 6.18, as this sample was not washed. For the as-spun yarn, the measured C/N ratio was 5.97, located between the calculated values of the powder and the spinning dope, which was caused by an incomplete removal of AcOH and acetate salts in the spinning baths. As expected, by applying standard washing procedure 1 in alkaline water, the C/N ratios of the adhesive and the fibers decreased (5.30 and 5.21, respectively) to the magnitude of the value of the pure chitosan powder (5.21), as AcOH was neutralized and washed out. However, this neutralization procedure resulted in the deformation of the substrate. To suppress this deformation in washing procedure 2, an ethanol solution was applied during scaffold fabrication. Elemental analysis suggested that scaffold washing procedure 2 removed most AcOH

Table 6. Electrostatic flocking in comparison to other textile technologies

Textile technology	Mechanical properties	Geometrical properties	Applications	Ref.
Weaving	High mechanical strength	Defined geometries, low SA:V	Nerve regeneration, vascular graft, fascia replacement/hernia repair, tendon/ligament repair	Aibibu et al.[18]
Knitting	Mechanical stability and elasticity, adapt to size changes	Defined geometries, low SA:V	Vascular grafts, nerve regeneration, dermal grafts, tendon regeneration, esophagus replacement, hernia repair, small joint reconstruction, calvarial bone healing	Aibibu et al.[18]
Braiding	High mechanical strength	Defined geometries, rope-like structures, low SA:V	Nerve regeneration, tendon/ligament repair	Aibibu et al.[18,36]
Nonwovens	Low mechanical strength	No defined geometries but adjustable pore size, low SA:V	Nerve regeneration, cartilage engineering, tendon/ligament repair	Aibibu et al.[18]
Electrospinning	Low mechanical strength	No defined geometries but adjustable pore size, high SA:V	Nerve regeneration, vascular grafts, bone regeneration, skin regeneration	Min et al.[37]
Electrostatic flocking	High compressive strength	Defined geometries, low SA:V	Cartilage engineering	This paper

from the fibers (C/N ratio of 5.28) and from the adhesive (C/N ratio of 5.51) as well, which made this washing procedure sufficient for the preparation of a pure chitosan scaffold.

Comparison to pure chitosan scaffolds from the literature

Different textile technologies can be applied for the manufacture of three-dimensional scaffold structures (Table 6). Making use of technologies like weaving, knitting, braiding, and electrostatic flocking, anisotropic structures with a defined spatial geometry can be fabricated. These structures are capable of withstanding high mechanical loads when fibers are oriented according to the distribution of forces, whereas electrospun structures and nonwovens have isotropic properties. However, electrospinning is the only manufacturing technique capable of producing nanofiber structures having a high SA:V.

In general, electrospinning of pure chitosan enables the fabrication of anisotropic and two-dimensional fiber mats,[37–40] making this technique suitable for the preparation of structures that may be applied as wound dressings. Even though fabrication of three-dimensional scaffolds by electrospinning methods was reported.[41] no three-dimensional and pure chitosan structures were under investigation in recent literature. Publications regarding the fabrication of mechanically stable three-dimensional scaffolds consisting of non-crosslinked chitosan are rare, despite its advantage for minimizing the risk of cytotoxicity of residual reactants or catalyst traces used for chitosan crosslinking. Isotropic chitosan fiber scaffolds, having a compressive strength of up to 53 kPa at a deformation of 50% were prepared by Ucar and colleagues.[42] It was highlighted that these microfibrous structures had a high SA:V and an interconnected porosity, but the pore sizes were not controllable. Jana and colleagues prepared freeze-dried and pure chitosan scaffolds to ensure biocompatibility.[43] The dry scaffolds had pore sizes ranging from 100 to 500 µm and a compressive strength of up to 1.74 MPa, whereas wet properties were not stated. Wang and colleagues prepared silica–chitosan hybrid scaffolds with a highly vertically oriented open porous structure by combining a sol–gel process and a freeze-casting technique.[44] Reference scaffolds prepared with chitosan only had a compressive strength of about 10 kPa at a deformation of 50%. Wan and colleagues produced hybrid scaffolds composed of polycaprolactone and chitosan by a particle-leaching technique.[45] If pure chitosan was applied in fabrication, the

compressive strength was 31 kPa at a deformation of 10%. The pore sizes were in the range 150–200 μm. Pourhaghgouy and Zamanian prepared unidirectional scaffolds composed of chitosan only.[46] The maximum compressive strength was found to be 110 kPa and the pore size was 90 μm. The chitosan scaffolds exhibited foam-like structures with pores that appeared to be hardly controllable, in some cases even completely uncontrollable. All those scaffolds were characterized by inter-pore openings, which were much smaller than the actual pore sizes hindering cell infiltration and nutrition flow. The wet compressive strengths of all those scaffolds and of the ones prepared for this work were in the same range. However, further mechanical investigation after in vitro cell cultivation is needed.

The technology of fiber flocking utilized in this work has proven to be advantageous over freeze drying and other methods, as the compressive strengths of up to 57 kPa at a deformation of 50% were comparatively high, while the pore and especially inter-pore sizes were large and controllable due to the manufacturing method. Furthermore, electrostatic flocking allows easy alteration of the material or the fiber composition, if needed. For instance, load-bearing fibers differing from those applied in this work are easily integrable within the flocked structure to enhance the compressive strength of the scaffold.

Conclusion

In the course of this work, fully resorbable scaffolds manufactured by electrostatic flocking were analyzed and an overview of the geometrical and the mechanical parameters of different scaffold types was given. The scaffolds were composed of a single material, namely chitosan, and featured a high compressive strength due to the vertically aligned flock fibers. The applied flocking technology enabled the preparation of chitosan scaffolds with high fiber density and high porosity. The scaffolds had pore sizes of up to 310 μm and compressive strength of up to 57 kPa at a deformation of 50%. The compressive strength of the scaffolds correlated with easily adjustable geometrical parameters. Hence, electrostatic flocking is proposed as a technique for the fabrication of tailor-made scaffolds for cartilage TE applications. However, the scaffold fabrication has to be optimized in order to reduce variation in scaffold properties, for example by technical modifications of the flocking device. Furthermore, a proper analysis method has to be developed to determine structural changes of the wet and swollen scaffolds during loading and unloading, for example by microcomputed tomography. Finally, an increased Young's modulus of the chitosan fibers in the wet state would be beneficial for the mechanical properties of the scaffolds, which in turn implies that non-toxic chitosan crosslinking methods may be necessary. This is, though, only the case if after cell culture the mechanical properties of the scaffolds turn out not to be satisfactory. Hence, further mechanical investigation after *in vitro* cell cultivation is needed.

Equations

Equations for spinning:

$$A_{CHS,0} = c_{vol} \cdot n \cdot \pi \cdot \left(\frac{d_s}{2}\right)^2 \tag{1.1}$$

where:

$A_{CHS,0}$ = flow rate area of chitosan
d_s = nozzle diameter
c_{vol} = volume concentration of chitosan in the spinning dope
n = nozzle count.

$$A_{CHS,6} = n \cdot \pi \cdot \left(\frac{d_6}{2}\right)^2 \tag{1.2}$$

where:

$A_{CHS,6}$ = area of chitosan yarn
d_6 = nominal single filament diameter.

$$v_0 = \frac{V_d \cdot n_p \cdot 4}{\pi \cdot d_s^2 \cdot n} \tag{1.3}$$

where:

v_0 = velocity at extrusion
v_d = displacement volume per revolution of pump
n_p = rotational speed of pump.

$$\dot{V}_{CHS} = const. = A_{CHS,0} \cdot v_0 = A_{CHS,6} \cdot v_6 \tag{1.4}$$

where:

$\dot{V}_{CHS}$ = volume flow chitosan
v_6 = velocity of sixth/last godet.

$$d_6 = 2 \cdot \sqrt{\frac{c_{vol} \cdot V_d \cdot n_p}{\pi \cdot n \cdot v_6}} \tag{1.5}$$

$$DR_i = \frac{v_i}{v_0}, \quad i = 0 \ldots 6 \tag{1.6}$$

where:

DR_i = drawing rate at a given godet
v_i = speed of a given godet
DR_6 = revealed the total drawing rate.

Equations for scaffold fabrication:

$$m_{f,sca} = m_s - m_{sub} \tag{2.1}$$

where:
$m_{f,\ sca}$ = weight of fibers within scaffold
m_s = weight scaffold structure
m_{sub} = weight of substrate.

$$y = \frac{m_{f,sca}}{m_{f,sie}} \tag{2.2}$$

where:
y = flocking yield
m_{sub} = weight of sieved fiber distributed onto electrode

$$fc_{tot} = \frac{4 \cdot m_{f,sca}}{\pi \cdot d_f^2 \cdot l_f \cdot \rho} \tag{2.3}$$

where:
fc_{tot} = flock fiber count within scaffold
l_f = measured flock fiber length (dry/wet)
d_f = measured flock fiber diameter (dry/wet)
ρ = chitosan density
(ρ set to 1.30 g/cm^3 for dry and to 1.12 g/cm^3 for wet state).

$$fc_g = \frac{4 \cdot fc_{tot}}{\pi \cdot d_{sca}^2} \tag{2.4}$$

where:
fc_g = gravimetrically determined flock fiber density
d_{sca} = scaffold diameter.

$$SA_f : \mathrm{V} = 2 \cdot \pi \cdot \frac{d_f}{2} \cdot fc_g \tag{2.5}$$

where:
SA_f: V = surface-area-to-volume ratio.

$$\phi = 1 - fc_g \cdot \pi \cdot \frac{d_f^2}{4} \tag{2.6}$$

where:
ϕ = porosity parallel to the plane of substrate.

$$d_{hex}^2 = \frac{\eta_h \cdot d_{sca}^2}{fc_{tot}} \tag{2.7}$$

where:
$\eta_h = \frac{\pi}{\sqrt{12}}$ = hexagonal packing density of circles within a circle.
d_{hex} = diameter of circles for hexagonal packing

$$p = d_{hex} - d_f \tag{2.8}$$

where:
p = pore size based on hexagonal packing.
Equations for Euler's critical load:

$$\sigma_E = \frac{\pi^3 \cdot E_{yarn} \cdot d_{f,wet}^2 \cdot fc_g}{256 \cdot l_{f,wet}^2} \tag{3}$$

where:
E_{wet} = Young's modulus of chitosan yarn in the wet state.

Declaration of conflicting interests

The authors declared no potential conflicts of interest with respect to the research, authorship, and/or publication of this article.

Funding

The authors disclosed receipt of the following financial support for the research, authorship, and/or publication of this article: This work was supported by the DFG (German Research Foundation) at the Technische Universität Dresden (Grant Numbers HU 2107/2-1, HO 1579/1-1 and GE 1133/16-1).

References

1. Nicolini AP, Carvalho RT, Dragone B, et al. Updates in biological therapies for knee injuries: full thickness cartilage defect. *Curr Rev Musculoskelet Med* 2014; 7: 256–262.
2. Makris EA, Gomoll AH, Malizos KN, et al. Repair and tissue engineering techniques for articular cartilage. *Nat Rev Rheumatol* 2015; 11: 21–34.
3. Hunziker EB, Lippuner K, Keel MJ, et al. An educational review of cartilage repair: precepts & practice – myths & misconceptions – progress & prospects. *Osteoarthr Cartil* 2015; 23: 334–350.
4. Johnstone B, Alini M, Cucchiarini M, et al. Tissue engineering for articular cartilage repair: the state of the art. *Eur Cell Mater* 2013; 25: 248–267.
5. Hutmacher DW. Scaffolds in tissue engineering bone and cartilage. *Biomaterials* 2000; 21: 2529–2543.
6. Gunn J and Zhang M. Polyblend nanofibers for biomedical applications: perspectives and challenges. *Trends Biotechnol* 2010; 28: 189–197.
7. Levengood SK and Zhang M. Chitosan-based scaffolds for bone tissue engineering. *J Mater Chem B* 2014; 2: 3161–3184.
8. Younes I and Rinaudo M. Chitin and chitosan preparation from marine sources: structure, properties and applications. *Mar Drugs* 2015; 13: 1133–1174.
9. Croisier F and Jérôme C. Chitosan-based biomaterials for tissue engineering. *Eur Polym J* 2013; 49: 780–792.
10. Suh JK and Matthew HW. Application of chitosan-based polysaccharide biomaterials in cartilage tissue engineering: a review. *Biomaterials* 2000; 21: 2589–2598.
11. Loh QL and Choong C. Three-dimensional scaffolds for tissue engineering applications: role of porosity and pore size. *Tissue Eng Part B Rev* 2013; 19: 485–502.

12. Talebian S, Mehrali M, Mohan S, et al. Chitosan (PEO)/bioactive glass hybrid nanofibers for bone tissue engineering. *RSC Advances* 2014; 4: 49144–49152.
13. Khanlou HM, Ang BC, Talebian S, et al. Electrospinning of polymethyl methacrylate nanofibers: optimization of processing parameters using the Taguchi design of experiments. *Text Res J* 2014; 85: 4356–4368.
14. Talebian S, Afifi AM and Khanlou HM. Fabrication and characterisation of chitosan/poly vinyl alcohol nanofibres via electrospinning. *Mater Res Innov* 2014; 18: 331–335.
15. Talebian S, Afifi AM, Hatami M, et al. Preparation and characterisation of electrospun silica nanofibres. *Mater Res Innov* 2014; 18: 510–514.
16. Zhao Y, Qiu Y, Wang W, et al. Preparation of nanofibers with renewable polymers and their application in wound dressing. *Int J Polym Sci* 2016; Article 4672839.
17. Tamayol A, Akbari M, Annabi N, et al. Fiber-based tissue engineering: progress, challenges, and opportunities. *Biotechnol Adv* 2013; 31: 669–687.
18. Aibibu D, Hild M, Wöltje M, et al. Textile cell-free scaffolds for in situ tissue engineering applications. *J Mater Sci Mater Med* 2016; 27: 1–20.
19. Walther A, Hoyer B, Springer A, et al. Novel textile scaffolds generated by flock technology for tissue engineering of bone and cartilage. *Materials* 2012; 5: 540–557.
20. Walther A, Bernhardt A, Pompe W, et al. Development of novel scaffolds for tissue engineering by flock technology. *Text Res J* 2007; 77: 892–899.
21. Balasubramanian P and Boccaccini AR. Bilayered bioactive glass scaffolds incorporating fibrous morphology by flock technology. *Mater Lett* 2015; 158: 313–316.
22. Vellayappan MV, Jaganathan SK and Supriyanto E. Review: unraveling the less explored flocking technology for tissue engineering scaffolds. *RSC Advances* 2015; 5: 73225–73240.
23. Steck E, Bertram H, Walther A, et al. Enhanced biochemical and biomechanical properties of scaffolds generated by flock technology for cartilage tissue engineering. *Tissue Eng Part A* 2010; 16: 3697–3707.
24. Gossla E, Tonndorf R, Bernhardt A, et al. Electrostatic flocking of chitosan fibers leads to highly porous, elastic and fully biodegradable anisotropic scaffolds. *Acta Biomater* 2016; 44: 267–276.
25. Li J, Du Y and Liang H. Influence of molecular parameters on the degradation of chitosan by a commercial enzyme. *Polym Degrad Stab* 2007; 92: 515–524.
26. Prasitsilp M, Jenwithisuk R, Kongsuwan K, et al. Cellular responses to chitosan in vitro: the importance of deacetylation. *J Mater Sci Mater Med* 2000; 11: 773–778.
27. Toskas G, Brünler R, Hund H, et al. Pure chitosan microfibres for biomedical applications. *Autex Res J* 2013; 13: 134–140.
28. Hild M, Toskas G, Aibibu D, et al. Chitosan/gelatin micro/nanofiber 3D composite scaffolds for regenerative medicine. *Compos Interface* 2014; 21: 301–308.
29. Shepherd DE and Seedhom BB. Thickness of human articular cartilage in joints of the lower limb. *Ann Rheum Dis* 1999; 58: 27–34.
30. Schindelin J, Arganda-Carreras I, Frise E, et al. Fiji: an open-source platform for biological-image analysis. *Nat Methods* 2012; 9: 676–682.
31. Cooper ML, Laxer JA and Hansbrough JF. The cytotoxic effects of commonly used topical antimicrobial agents on human fibroblasts and keratinocytes. *J Trauma Acute Care Sur* 1991; 31: 775–784.
32. Lineaweaver W, McMorris S, Soucy D, et al. Cellular and bacterial toxicities of topical antimicrobials. *Plast Reconstr Surg* 1985; 75: 394–396.
33. Knaul JZ, Hudson SM and Creber KA. Improved mechanical properties of chitosan fibers. *J Appl Polym Sci* 1999; 72: 1721–1732.
34. Notin L, Viton C, David L, et al. Morphology and mechanical properties of chitosan fibers obtained by gel-spinning: influence of the dry-jet-stretching step and ageing. *Acta Biomater* 2006; 2: 387–402.
35. Kerin AJ, Wisnom MR and Adams MA. The compressive strength of articular cartilage. *Proc Inst Mech Eng H J Eng Med* 1998; 212: 273–280.
36. Aibibu D, Hild M and Cherif C. An overview of braiding structure in medical textile: fiber-based implants and tissue engineering. In: Kyosev Y (ed.) *Advances in braiding technology: Specialized techniques and applications*. Cambridge: Woodhead Publishing, 2016.
37. Min BM, Lee SW, Lim JN, et al. Chitin and chitosan nanofibers: electrospinning of chitin and deacetylation of chitin nanofibers. *Polymer* 2004; 45: 7137–7142.
38. Geng X, Kwon OH and Jang J. Electrospinning of chitosan dissolved in concentrated acetic acid solution. *Biomaterials* 2005; 26: 5427–5432.
39. Haider S and Park SY. Preparation of the electrospun chitosan nanofibers and their applications to the adsorption of Cu (II) and Pb (II) ions from an aqueous solution. *J Membr Sci* 2009; 328: 90–96.
40. Homayoni H, Ravandi SA and Valizadeh M. Electrospinning of chitosan nanofibers: processing optimization. *Carbohydr Polym* 2009; 77: 656–661.
41. Sun B, Long YZ, Zhang HD, et al. Advances in three-dimensional nanofibrous macrostructures via electrospinning. *Prog Polym Sci* 2014; 39: 862–890.
42. Ucar S, Yilgor P, Hasirci V, et al. Chitosan-based wet-spun scaffolds for bioactive agent delivery. *J Appl Polym Sci* 2013; 130: 3759–3769.
43. Jana S, Florczyk SJ, Leung M, et al. High-strength pure porous chitosan scaffolds for tissue engineering. *J Mater Chem* 2012; 22: 6291–6299.
44. Wang D, Romer F, Connell L, et al. Highly flexible silica/chitosan hybrid scaffolds with oriented pores for tissue regeneration. *J Mater Chem B* 2015; 3: 7560–7576.
45. Wan Y, Wu H, Cao X, et al. Compressive mechanical properties and biodegradability of porous poly(caprolactone)/chitosan scaffolds. *Polym Degrad Stabil* 2008; 93: 1736–1741.
46. Pourhaghgouy M and Zamanian A. Physical and mechanical properties of the fully interconnected chitosan ice-templated scaffolds. *J Appl Polym Sci* 2015; 132: 41476. doi: 10.1002/app.41476.